Physics Procedia

Volume 75, 2015, Pages 62–69

20th International Conference on Magnetism

Defect induced enhanced low field magnetoresistance and photoresponse in $Pr_{0.6}Ca_{0.4}MnO_3$ thin films

Tomi Elovaara[1], Sayani Majumdar[1,2], Hannu Huhtinen[1], and Petriina Paturi[1]

[1] Wihuri Physical Laboratory, Department of Physics and Astronomy, University of Turku, FI-20014 Turku, Finland tomi.elovaara@utu.fi

[2] Nanomagnetism and Spintronics Group, Department of Applied Physics, Aalto University School of Science, P.O. Box 15100, FI-00076 Aalto, Finland

Abstract

We have investigated the effect of grain boundary related defects on the electronic transport properties of the colossal magnetoresistive low bandwidth manganite $Pr_{0.6}Ca_{0.4}MnO_3$ (PCMO) thin films. A series of PCMO films were prepared by pulsed laser deposition method on MgO and STO substrates. Characterizations of the structural, magnetic and magneto-transport properties show that the films prepared on MgO substrate contain higher amount of structural defects and with decreasing deposition temperature an increasing amount of different crystal orientations as the level of texturing decreases. According to the low field magnetoresistance (MR) measurements, the poorly textured samples display an increased low field MR due to a grain boundary tunneling effect at low temperatures compared to the fully textured PCMO film on STO substrate. However, in spite of the level of texturing, all the samples showed a colossal magnetoresistive insulator to metal switching of almost eight orders of magnitude at low temperatures. The magnetic field required for insulator to metal transition (IMT) is much higher in PCMO samples with more structural defects. However, IMT field could be reduced over 3 T by illuminating the sample.

Keywords: low bandwidth manganite, thin film, grain boundaries, low field magnetoresistance, colossal magnetophotoresistance

1 Introduction

Strongly correlated electron systems often exhibit very strong interaction between the structural and electronic degrees of freedom that lead to exotic magnetic and electronic properties. For the low bandwidth manganite $Pr_{1-x}Ca_xMnO_3$, these properties are such as colossal magnetoresistance [1, 2], charge-ordering (CO) [3], first order irreversible metamagnetic transition [4], colossal magnetophotoresistance [5] and large magnetocaloric effects [6]. These exciting magnetic and transport properties often results from strong competition between different phase-separated regimes [7]. PCMO has a highly distorted orthorombic perovskite crystal structure

Selection and peer-review under responsibility of the Scientific Programme Committee of ICM 2015

doi:10.1016/j.phpro.2015.12.010

with distorted oxygen octahedra around Mn^{3+} ions due to Jahn-Teller (JT) effect. Therefore, hopping of e_g electrons between the Mn^{3+} and Mn^{4+} is restricted making it insulating in the entire hole doping range. The localized e_g electrons induce the formation of charge and orbital order (CO/OO) state with the Ca concentration of $0.3 \leq x \leq 0.7$. An external magnetic or electric field, as well as an ambient pressure or an optical excitation [5, 8, 9, 10, 11] can modify the magnetic ordering and electronic properties of the CO state of PCMO by changing the Mn–O–Mn bond angle, increasing the hopping amplitude of electrons *i.e* mobility, in the double-exchange (DE) mechanism [12, 13]. This effectively enhances ferromagnetic (FM) ordering reducing the resistivity of PCMO and leading to colossal magnetoresistance effect (CMR). To harness these intriguing phenomena for potential resistive memory applications of PCMO, it is important to know how the preparation process affects the different elements of crystal structure and further the transport properties of thin films.

In the present work, we study the transport properties of PCMO thin films of different crystallinity by preparing films on different substrates using optimized pulsed laser deposition (PLD) parameters. The thin film on single crystalline substrate $SrTiO_3$ (STO) showed complete epitaxial growth, with only low angle grain boundary (GB) related defects. Depending on deposition conditions, the films grown on MgO substrate showed only a partial texturing of the film with high angle GB related defects and even polycrystalline growth.

2 Experimental Methods

2.1 Sample preparation and characterization

The PCMO ($x = 0.4$) films were prepared by pulsed laser deposition (PLD) method using an excimer XeCl 308 nm laser with laser fluence 1.3 Jcm^{-2}, a pulse duration of 25 ns and a repetition rate of 5 Hz. The PCMO films were grown on two different substrate materials, (100) MgO and (100) $SrTiO_3$ (STO), having different lattice mismatch values of 8.9 % and 1.8 % (tensile strain), respectively, compared to PCMO bulk material. During the deposition, the flowing oxygen pressure on the chamber was $p = 0.2$ torr. In order to affect the structural properties of the films grown on MgO substrates, deposition temperatures of 600 and 750 °C were used. Hence, the samples on MgO are called MgO-600 and MgO-750. For the thin film grown on STO substrate, an already optimized deposition temperatures of 500 °C were used (called STO-500) [14]. All the films had an *in situ* post-annealing treatment at the deposition temperature in atmospheric pressure of oxygen for 10 min with heating and cooling rates of 25 °C/min. The thickness of the film on STO substrate was ≈ 110 nm as defined using atomic force microscopy over an etched edge. For the films deposited on MgO substrates with higher lattice mismatch, the thicknesses were ≈ 70 nm as defined by X-ray reflectometry.

The structural properties of the films were determined by XRD measured with a Philips X'Pert Pro MPD system with an incident beam x-ray mirror, Schulz texture goniometer and PixCel 1D detector. The phase purity of the films was confirmed from the $\theta - 2\theta$ scans in out-of-plane ($0b0$) direction. The lattice parameters were determined from detailed 2D (ϕ, 2θ) texture scans of PCMO (112)/(031) peaks for films on STO, and (121) and (040) peaks for films on MgO.

2.2 Magnetic and magnetoresistive measurements

The magnetic measurements were made with a Quantum Design MPMS SQUID magnetometer measuring the temperature dependence of zero-field-cooled (ZFC) and field-cooled (FC) magne-

tizations in the field of 100 mT. The virgin magnetizations, where the magnetic field is applied for the first time, were measured as a function of the external magnetic field B and magnetic hysteresis curves were recorded in a field of $B = \pm 5$ T at temperatures of 10, 30, 50, 70, 100 and 250 K. The external field B was always oriented along the planes of the films, *i.e.* along the PCMO [101] axis.

The magnetoresistive measurements were executed with a standard two point connection in PPMS magnetometer connected to the Keithley 6487 picoammeter. The virgin magnetoresistivity followed by the hysteresis loop measurements were recorded in a field of $B = \pm 8$ T at temperatures of 10, 20, 30, 50, 70, 100 and 300 K. The external field B was always perpendicular to the planes of the films, *i.e.* along the PCMO [010] axis. The copper wiring was made to the surface of film with indium brazing. The distance between the connectors was around 3.5 mm. All the measurements were made in dark or under photoexcitation keeping the other experimental conditions unchanged. Photoinduced measurements were performed with a home-made fibreoptic sample holder attached to the PPMS magnetometer where the laser spot covered the whole PCMO film. The used light source was AlGaInP laser diode working at $\lambda =$ 658 nm (1.88 eV) with the total output density of ≈ 0.4 mWmm^{-2} on the sample surface.

During the magnetoresistivity measurements, the voltage is linearly changed so that the current stayed constant at 2 μA between voltages 0.1 and 200 V. The corresponding resistances are $5 \cdot 10^4$ Ω (0.1 V) and 10^8 Ω (200 V). In the resistivity range under $5 \cdot 10^4$ Ω and over 10^8 Ω, the measuring mode changes on the fly to the constant voltage mode where the voltage stays at 0.1 and 200 V, respectively. The current was measured in the resistivity range where the constant voltage mode was used. However, the current is always kept below 2 mA at low resistivity regions to avoid the colossal electroresistant effect [15].

3 Results and discussion

3.1 Structural characterization

The structural characterization of the thin films was made by XRD measurements. The measured 2θ scans for films grown on STO showed only $(0k0)$ peaks of the PCMO in addition to the substrate $(l00)$ peaks indicating single phase film with (010) crystal orientation *i.e.*, with [010] axis perpendicular to the substrate plane. The 2θ diffractograms for films deposited on MgO substrates with higher lattice mismatch are presented in figure 1(a), from which we can observe that for sample MgO-600 no PCMO peaks can be detected indicating poorly crystalline film. For sample MgO-750, there are visible extra peaks (121) and (242) in addition to normal $(0k0)$ peaks, indicating at least two different crystal orientations.

The pole figures, attained from the texture scans of the PCMO peak (121) reflections with relative intensities for films on MgO, are given on the right side of figure 1(a). Again, the sample MgO-600 does not show any visible peaks indicating polycrystalline film and the sample MgO-750 shows three different preferred crystalline orientations where [010], [220] and [121]-directions are situated out-of-plane from the face of the film surface. In addition, parts of these crystal orientations are also rotated in-plane. However, according to the peak intensities the most probable orientation is to have the lattice vector b out-of-plane. This means that in the thin films grown on MgO substrate there is high angle GBs between the different crystal orientations. It is evident that the smaller lattice mismatch between PCMO bulk and STO substrate compared to MgO substrate induce better crystallization of PCMO thin films on STO substrate.

From the $2\theta - \phi$ scans, the crystalline quality, including the presence of possible defects

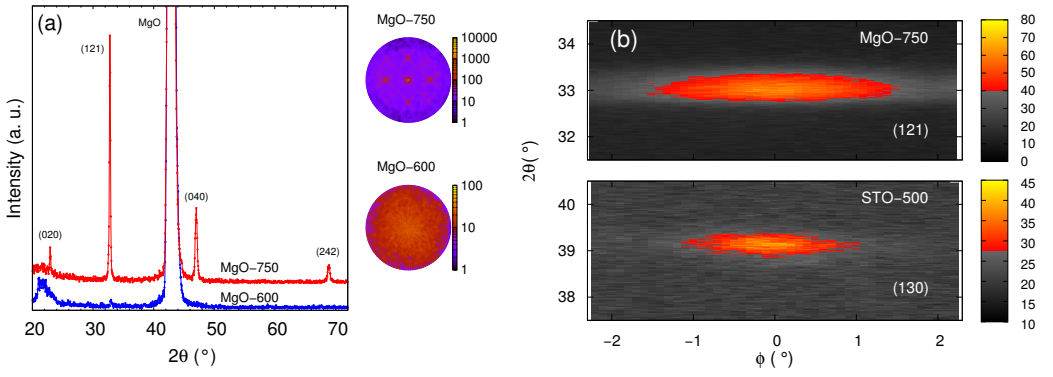

Figure 1: The x-ray 2θ diffractograms at room temperature with identified peaks of the PCMO and the pole figures of the texture scans with relative intensities measured at $2\theta = 32.8°$ for the (121) peak of PCMO for films deposited on MgO substrates (a). The 2θ and ϕ scans with equivalent x and y ranges of the peaks (121) and (130) for MgO-750 and STO-500 samples, respectively (b).

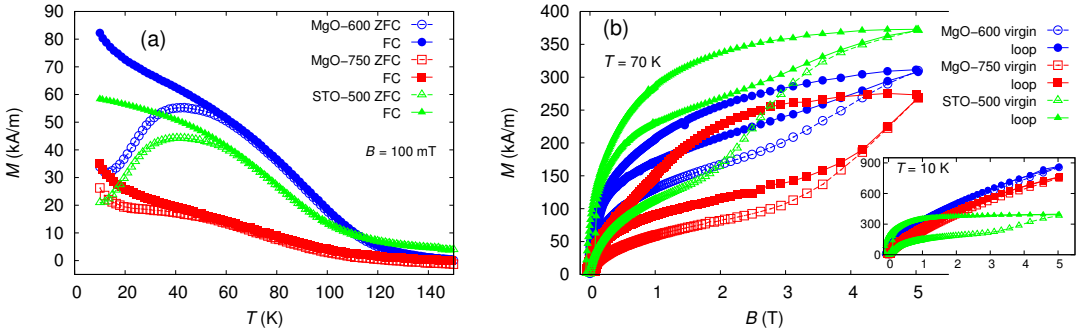

Figure 2: Temperature dependence of the M_{ZFC} and M_{FC} magnetizations ($B = 100$ mT) for PCMO films deposited on MgO and STO substrates (a). The virgin and hysteresis loop measurements are shown only from the positive magnetic field side, and measured at 70 K for all the samples (b). The insets show the same measurement at 10 K.

such grain boundaries (GBs) that broaden the XRD peaks, can be evaluated. As can be seen from figure 1(b), the peak (121) is very broad in ϕ-direction for sample MgO-750, indicating much more low angle GBs when compared to the STO-500 sample. In the figure 1(b), the colour palette has high contrast between low and high intensities, changing at the midpoint of intensity, highlighting the full width half maximum (FWHM) of the peaks.

3.2 Magnetic properties

The temperature dependence of the magnetization $M(T)$ is presented in figure 2(a) which shows a thermomagnetic irreversibility for all the samples, indicating competing FM and AFM

clusters at low temperatures. The measured magnetization value has been scaled with the volume of the films. The lowest magnetization was found on sample with highest deposition temperature at 750 °C, indicating highest amount of AFM clusters in the sample.

The virgin and hysteresis loop measurements at 10 K, presented in figure 2(b) inset, show a high training effect for film on STO where the slope of the virgin curve increases in high field range and the following loop measurement stays in the higher magnetization level without any hysteresis. This behaviour indicates a persistent metamagnetic AFM to FM transition at 10 K with moderate applied magnetic field for STO-500 sample [4, 14]. For films on MgO, the maximum applied magnetic field of 5 T is not sufficient to induce the metamagnetic AFM to FM transition at 10 K. The virgin curves at 70 K, presented at figure 2(b), show the metamagnetic transition for all the samples indicating a lower required magnetic field for AFM to FM transition at higher temperatures. However, this metamagnetic transition disappears above the critical temperature $T_N \approx 100$ K for all the samples. Also the loop curves in figure 2 show a clear hysteresis for all the samples, indicating that the higher temperature relaxes the sample from the FM metastate back to the initial AFM state when the magnetic field is returned to zero. According to these magnetic and XRD, data it is evident that the imperfections in the crystal structure of the MgO samples increase the required field for AFM to FM transition.

3.3 Transport measurements

The Magnetoresistive virgin measurements, where the magnetic field is applied for the first time, are presented in figure 3(a-b) in dark and under illumination for all the samples. The IMT, where the resistance of the sample drops around 5 - 9 decades depending on the sample, is visible for all the samples. The IMT is closely related to the metamagnetic AFM to FM transition and hence the magnetoresistive virgin measurements at 10 K correspond very well to the magnetic virgin measurements at 10 K. The higher resistance in the metallic (low resistance) state in MgO samples can be caused by the lower thickness of the samples. Also the higher resistivity is expected, considering maximum structural disorder in the unit cells and the presence of higher amount of low angle GBs in MgO films, leading to higher charge carrier scattering at the GBs, and therefore, decreasing the conductivity of the sample. This also affects the overall resistance change in IMT, because the resistance of 10^{13} Ω is within the upper limit of the measurement. Also, the light reduces the required magnetic field for IMT and the effect of light seems to be stronger in the films on MgO reducing the IMT field over 3 tesla. Similar phenomenon is previously observed by Elovaara *et. al.* [5]. For the MgO samples with high angle GBs and higher amount of low angle GBs, the IMT is more gradual and the required magnetic field for it is much higher compared to the STO-500 sample with low amount of low angle GBs. These results are in line with the magnetic measurements and indicate that the imperfections in crystal structure affect also the IMT transition.

The IMT transition at several temperatures for sample MgO-600 is presented in the figure 3(b) and the temperature dependence of IMT field for all the samples is presented in the figure 3(c). For all the samples, increasing temperature decreases the IMT field, which is again in agreement with magnetic virgin measurements. Hence, the effect of illumination and heating is similar for all the samples. Also, the light induced reduction of the IMT field decreases with increasing temperature. However, as can be seen from the figure 3(c), the laser light with the total output density of ≈ 0.4 mW/mm^2 on the sample surface is not enough to heat the sample to solely explain the illumination effect. The heating effect of the laser in this measurement setup has also been previously discussed by Elovaara *et al.* [5]. The photons of 1.88 eV energy excite the Mn^{3+} e_g electron relaxing the Jahn-Teller distortion of the surrounding oxygen

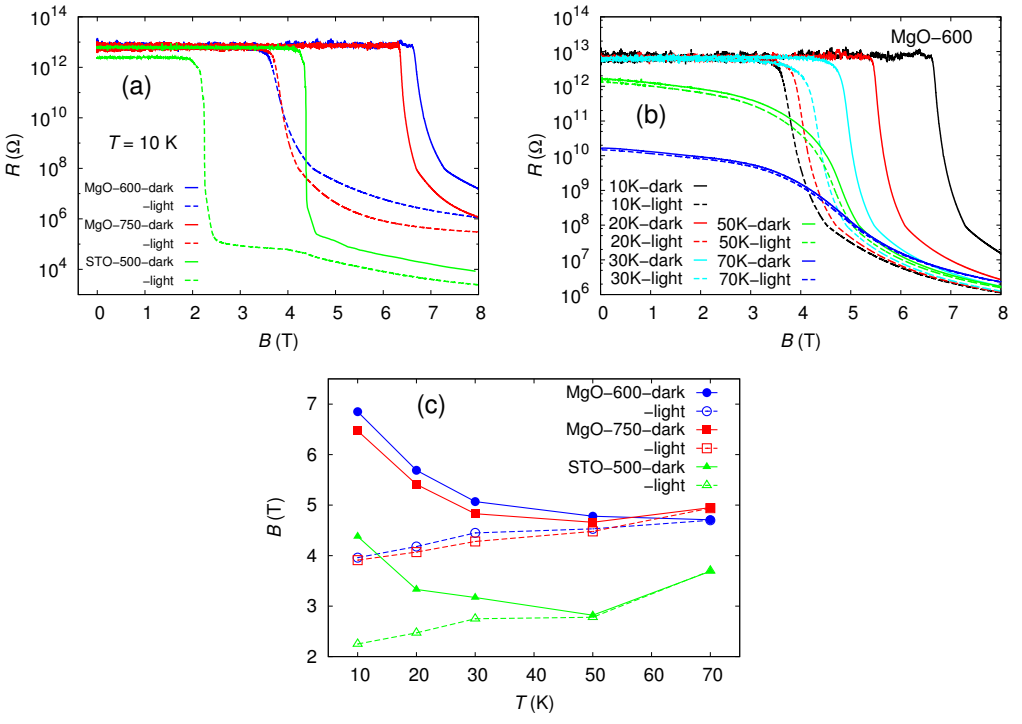

Figure 3: Resistance of the samples measured at 10 K in dark (solid) and under illumination (dashed) while the external magnetic field is slowly risen to 8 T for the first time (virgin) for all the films (a). Magnetoresistive virgin measurement in different temperatures for sample MgO-600 (b). The temperature dependences of IMT field in dark and under illumination for all the samples (c). The IMT field is measured from the middle of the IMT transition.

octahedra and exciting the optical phonon modes and simultaneously inducing the melting of the charge and orbital ordering [16]. Similarly, the heating of the samples lowers the IMT field as the heating excites thermal phonons of the crystal lattice weakening the CO state [5].

The IMT is also achieved solely with illumination when the background magnetic field is adjusted between IMT fields in dark and under illumination. We have reported this kind of magnetically biased magnetophotoresistance earlier for PCMO thin films [5].

After the magnetoresistive virgin measurements, loop measurements were performed (figure 4 insets). These are in agreement with the magnetic measurements as the resistivity does not return to its initial value after removing the magnetic field, hence the metallic (FM) state is persistent at 10 K. Also, the resistance hysteresis in the loop measurements increases with the temperature (not shown here) as the sample flips back to the more insulating (AFM) phase at higher temperatures. The samples with more low angle GBs display high low field magnetoresistance (LFMR) in the metallic phase as presented in figure 4. Similar defects and GB induced large LFMR effect was observed before in half metallic oxide LSMO by Majumdar *et al.* [17]. The LFMR observed from the resistance hysteresis loops in the metallic phase at low temperatures with appearance of two peaks support the presence of GB tunneling MR in all the films [17, 18]. MR at low fields can be understood in terms of tunneling of spin polarized

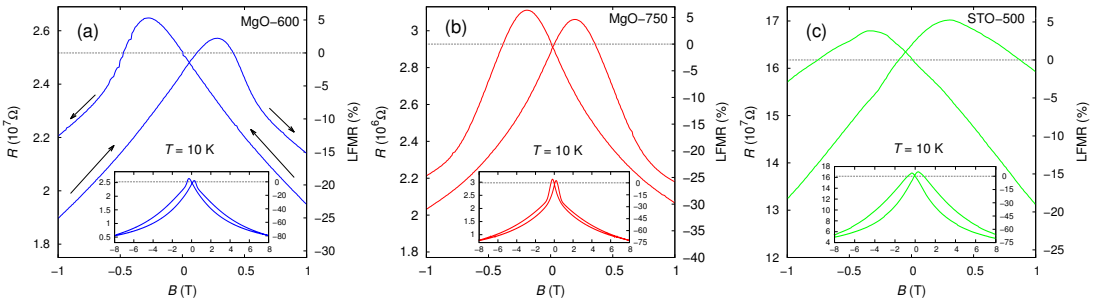

Figure 4: Magnetoresistive loops at 10 K measured from 8 T to -8 T and back in dark for the samples MgO-600 (a), MgO-750 (b) and STO-500 (c) with calculated low field magnetoresistance (LFMR) percentage $[(R_H - R_{0T-dark})/R_{0T-dark}] \cdot 100\%$.

conduction electrons between FM grains separated by the GBs. Upon sweeping the magnetic field, relative orientation of the magnetic moment between the FM grains changes and the probability of electrons tunneling between grains separated by GBs gets modified. This shows up in a change in sample resistance showing a maximum after the background magnetic field direction is changed, when the magnetic disorder between the grains is highest. While the background magnetic field is further increased, the magnetic moments between grains starts to align again inducing lower resistance. This magnetic field induced drop in resistivity, after the maximum peak, is observed to be substantially more prominent in samples with higher amount of GBs where the charge carriers suffer more scattering which upon application of a magnetic field reduces leading to larger LFMR. The smaller LFMR effect in STO-500 sample leads to large irreversibility effect which is observed even in high magnetic field regime. The LFMR effect is the highest at 10 K and decreases with increasing temperature in every sample.

4 Conclusion

In conclusion, we have shown that depending on the GB related defects in the PCMO thin films, the LFMR and the magnetic field required for IMT can be modified. Even though the differences in crystal structures between these films were large, all the samples showed thermomagnetic irreversibility, persistent metamagnetic AFM to FM transition, which is closely related to IMT transition, and colossal magnetophotoresistance. Surprisingly, even the polycrystalline film on MgO substrate showed similar colossal magnetophotoresistance and LFMR phenomenon as the textured films. This is a nice result in terms of technological applications, because now the growth parameters and the selection of the substrates are not so crucial as the film does not have to be single crystalline to maintain its properties. However, in the better crystalline film the IMT occur at much lower magnetic field.

Acknowledgements

The Jenny and Antti Wihuri Foundation is acknowledged for financial support.

References

[1] S. Jin, R. C. Sherwood, E. M. Gyorgy, T. H. Tiefel, R. B. van Dover, and S. Nakahara. *Appl. Phys. Lett.*, 54:584, 1988.

[2] A.-M. Haghiri-Gosnet and J.-P. Renard. *J. Phys. D.:Appl. Phys.*, 36:R127, 2003.

[3] Y. Tokura. Gordon and Breach Science, New York, 2000.

[4] T. Elovaara, H. Huhtinen, S. Majumdar, and P. Paturi. *J. Phys. Cond. Mat.*, 24:216002, 2012.

[5] T. Elovaara, S. Majumdar, H. Huhtinen, and P. Paturi. *Adv. Funct. Mater. accepted*, 6/2015.

[6] V. S. Kolat, T. Izgi, A. O. Kaya, N. Bayri, H. Gencer, and S. Atalay. *J. Magn. and Magn. Mater.*, 322:427, 2010.

[7] A. Dagotto, T. Hotta, and A. Moreo. *Physics Reports*, 344:1, 2001.

[8] K. Miyano, T. Tanaka, Y. Tomioka, and Y. Tokura. *Phys. Rev. Lett.*, 78:4257, 1997.

[9] M. Fiebig, K. Miyano, T. Satoh, Y. Tomioka, and Y. Tokura. *Phys. Rev. B*, 60:7944, 1999.

[10] S. Majumdar, H. Huhtinen, M. Svedberg, P. Paturi, S. Granroth, and K. Kooser. *J. Phys. Cond. Mat.*, 23:466002, 2011.

[11] S. Majumdar, T. Elovaara, H. Huhtinen, S. Granroth, and P. Paturi. *J. Appl. Phys.*, 113:063906, 2013.

[12] C. Zener. *Phys. Rev.*, 82:403, 1951.

[13] G. H. Jonker and J. H. van Santen. *Physica*, 16:337–349, 1950.

[14] T. Elovaara, T. Ahlqvist, S. Majumdar, H. Huhtinen, and P. Paturi. *J. Magn. and Magn. Mater.*, 381:194, 2015.

[15] Ch. Jooss, R. Warthmann, A. Forkl, and H. Kronmüller. *Physica C*, 199:215, 1998.

[16] P. Beaud, A. Caviezel, S. O. Mariager, L. Rettig, G. Ingold, C. Dornes, S.-W. Huang, J. A. Johnson, M. Radovic, T. Huber, T. Kubacka, A. Ferrer, H. T. Lemke, M. Chollet, D. Zhu, J. M. Glownia, M. Sikorski, A. Robert, H. Wadati, M. Nakamura, M. Kawasaki, Y. Tokura, S. L. Johnson, U. Staub. *Nature Materials*, 13:923, 2014.

[17] S. Majumdar, H. Huhtinen, P. Paturi, and H. S. Majumdar. *J. Mater. Sci.*, 48:2115, 2013.

[18] A. Gupta, G. Q. Gong, G. Xiao, P. R. Duncombe, P. Lecoeur, P. Trouilloud, Y. Y. Wang, V. P. Dravid, and J. Z. Sun. *Phys. Rev. B*, 54:R15629, 1996.